Research Square

Preprints are preliminary reports that have not undergone peer review.
They should not be considered conclusive, used to inform clinical practice,
or referenced by the media as validated information.

Robust OFDM Receiver using null-subcarrier-aided OMP with MCC based equalization for QCA/VLSI-induced non-Gaussian noise

Sachin Aralikatti

sachin.a@cmrit.ac.in

CMR Institute of Technology

Shridhar N

CMR Institute of Technology

Rangeet Mitra

CMR Institute of Technology

Research Article

Keywords:

Posted Date: November 4th, 2026

DOI: https://doi.org/10.21203/rs.3.rs-9963549/v1

License: This work is licensed under a Creative Commons Attribution 4.0 International License.
Read Full License

Additional Declarations: No competing interests reported.

Robust OFDM Receiver using null-subcarrier-aided OMP with MCC based equalization for QCA/VLSI-induced non-Gaussian noise

Sachin Aralikatti[1*], Shridhar N[2] and Rangeet Mitra[3]

[1,2,3]Department of ECE, CMRIT Bengaluru, Karnataka, 560037, India, Visvesvaraya Technological University, Belagavi – 590018, Bengaluru, 560037, Karnataka, India.

*Corresponding author(s). E-mail(s): sachin.a@cmrit.ac.in ;
Contributing authors: sridhar.n@cmrit.ac.in; rangeet.m@cmrit.ac.in;

Abstract

The fast Fourier transform (FFT) is a widely celebrated algorithm in the domain of signal processing with applications such as orthogonal frequency division multiplexing (OFDM), for indoor wireless LAN scenarios and LTE downlink. However, analytical studies in this paper, lead us to conclude that FFT-implementations based on quantum cellular automata (QCA), under certain conditions, are impaired by $\boldsymbol{\alpha}$-stable noises due to miniaturization with large density of gates per unit area. These stable distributed noises impede applications which use QCA based FFT-like modules. This paper introduces the use of orthogonal matching pursuit (OMP) based denoising in conjunction with maximum correntropy (MCC) based information theoretic equalization for QCA-FFT. The performance-evaluation for the proposed QCA-FFT with OMP/MCC based denoising is presented for two case-studies, namely, 802.11a wireless local area network OFDM standard, and for higher order OFDM in LTE downlink, where large gains in BER performance is reported for the proposed algorithm over QCA based FFT computations.

Keywords: QCA Statistical Modeling Denoising Information Theoretic Learningfast-Fourier transform.

1 Introduction

The rapid growth of digital signal processing (DSP) applications in multimedia systems, wireless communications, biomedical imaging, and information security has significantly increased the demand for high-performance and energy-efficient computational architectures. Conventional Complementary Metal–Oxide–Semiconductor (CMOS) technology has served as the backbone of integrated circuit design for several decades. However, as device dimensions approach the nanometer scale, CMOS technology faces severe physical limitations including short-channel effects, increased leakage currents, thermal dissipation, and quantum mechanical phenomena. These limitations restrict further transistor scaling and threaten the continuation of Moore's law, thereby motivating the exploration of alternative computing paradigms capable of achieving higher device density and improved energy efficiency [1–3].

Among the emerging post-CMOS technologies, Quantum-dot Cellular Automata (QCA) has emerged as a promising nanocomputing paradigm. As compared to conventional CMOS circuits, which rely on current flow through transistors, QCA represents binary information through polarization states of electrons inside quantum-dot cells. Computations are performed via Coulombic interactions between neighboring cells instead of charge transport, which enables currentless switching and ultra-low energy dissipation. This electrostatic interaction mechanism allows for operation at extremely high device densities and switching speeds while minimizing resistive power loss. In addition, the inherent clocking mechanism in QCA enables pipelined data propagation through sequential zones, which makes the technology particularly suitable for high-performance nanoscale computation [4, 5].

1.1 Limitations of Classical QCA

In spite of aforementioned advantages, the reliability of QCA circuits remains a major challenge for practical large-scale implementations. At nanoscale dimensions, QCA circuits are highly sensitive to fabrication defects, thermal fluctuations, clocking disturbances, cell misalignment, and environmental noise. These disturbances introduce uncertainty in the polarization states of QCA cells and leads to error-propagation through logic networks, thereby degrading computational accuracy. As circuit complexity increases, error accumulation negatively affects the reliability of arithmetic-intensive operations that are commonly used in digital signal processing architectures.

A notable limitation in conventional digital circuit design arises from irreversible computation. According to Landauer's principle, the erasure of one bit of information inevitably dissipates a minimum energy of K*T*ln (2) joules, where k denotes Boltzmann's constant and T represents the absolute temperature [6]. This thermodynamic limit applies regardless of the underlying computing technology and becomes increasingly significant in nanoscale circuits. Reversible logic provides an attractive solution to this challenge by establishing an injective correspondence between input and output states, thereby preserving information during computation. When implemented with adiabatic switching mechanisms, reversible circuits can theoretically achieve near-zero energy dissipation. Thus, this integration of reversible logic with

QCA technology offers a powerful framework for designing ultra-low-power nanoscale computing architectures with improved thermodynamic efficiency [7, 8].

1.2 Potential of QCA circuits in DFT Systems

Reversible QCA circuits have emerged as a promising solution for implementing complex operations required in DSP systems. Many advanced signal processing applications rely heavily on arithmetic operations such as addition, subtraction, and complex multiplication, which in-turn rely on logic gates. For example, these arithmetic blocks serve as the fundamental building components for Discrete Orthogonal Transform (DOT) architectures [9–15], including the Discrete Cosine Transform (DCT), Discrete Fourier Transform (DFT), and Fast Fourier Transform (FFT). Such transforms are extensively used in wireless communication systems like orthogonal frequency division multiplexing (OFDM) [16].

1.3 General Motivation for Information Theoretic Learning Based Algorithms for Parameter-Estimation

However, the reliability of transform architectures implemented using nanoscale technologies such as QCA can be significantly affected by circuit-level noise disturbances. Traditional signal processing models typically assume Gaussian noise distributions. In practical nanoscale systems, however, noise often exhibits impulsive characteristics and heavy-tailed statistical behavior. For example, alpha-stable distributions are frequently used to model additive degradations in impulsive noise environments. Such disturbances can propagate through arithmetic circuits and significantly degrade system-level performance metrics such as Bit Error Rate (BER) in communication systems employing FFT-based signal processing blocks.

To address these challenges, this work proposes a noise-resilient computational framework incorporating denoising-aware arithmetic blocks based on the maximum correntropy (MCC) principle. Unlike conventional error minimization approaches such as Mean Square Error (MSE), which assume Gaussian noise distributions, the MCC criterion minimizes the outliers of the error distribution (such as the error-outputs of orthogonal matching pursuit (OMP) and demonstrates superior robustness in environments characterized by generic impulsive and non-Gaussian noise. The MCC algorithm belongs to the class of Information Theoretic Learning (ITL) methods, evaluates the statistical structure of the error signal and tends to the Renyi -α information potential for $\alpha = 2$ [17]. By maximising the correntropy, the algorithm effectively suppresses noise and improves signal reliability in generic non-Gaussian environments.

1.4 Justification for Model of Noisy Gates Impaired by Stable Distribution in QCA

As QCA devices are aggressively miniaturized, the reliable localization of electrons within quantum dots becomes increasingly sensitive to thermal fluctuations, charge variations, and environmental disturbances. In particular, when the thermal energy (kT) approaches the kink energy (Ek), the polarization of QCA cells weakens, resulting

in unstable logic states and increased probability of computational errors [18]. These effects are further exacerbated by reduced energy barriers in nanoscale structures, which make electron tunneling and polarization flipping more susceptible to noise. In addition to thermal noise, leakage-like effects arise due to unintended electrostatic interactions between neighboring cells. Since QCA circuits rely on Coulombic coupling rather than current flow, the absence of electrical isolation can lead to undesired inter-cell interference, crosstalk, and signal degradation [19].

As device density increases, proximity effects and interconnect interactions further intensify these disturbances, significantly impacting signal integrity and circuit reliability. Fabrication imperfections also play a critical role in noise generation in QCA systems. Variations such as cell misalignment, displacement, omission, and intercellular spacing errors can alter electrostatic coupling between cells, leading to incorrect polarization states and faulty logic behavior [20]. At nanoscale dimensions, even minor structural deviations can cause significant functional degradation, highlighting the strong dependence of QCA operation on precise geometric alignment. Moreover, energy dissipation mechanisms, including phonon interactions and environmental coupling, contribute to signal attenuation during information propagation. Without periodic restoration of signal energy through clocking mechanisms, logic states may degrade as they propagate across multiple stages, further amplifying noise effects [21]. In this context, the polarization equation (assuming an Ising Potts model) in the scenario affected by cross-talk between several nodes is given as:

$$p_i = \tanh\left[\frac{\sum_j J_{ij} p_j}{k_B T}\right], \tag{1}$$

where J denotes the neighborhood coupling matrix, k_B is the Boltzmann constant, T is the temperature, and p_j denotes the polarizations of the neighborhood circuits [4, 22]. In general, if the sum in $\sum_j J_{ij} p_j$ converges, it is inferred from the above coupling equation that the additive noise is Gaussian; else, by the generalized central limit theorem, the additive couplings will be an α-stable distribution. Notably, $\alpha \in [1, 2]$, where $\alpha = 1$ denotes the most severe kind of additive noise and $\alpha = 2$ denotes the Gaussian distribution [23].

Major Contributions of This Work: Based on this review, the major contributions of this work are outlined as follows:

- The derivation/fitting of the distribution of additive noise in highly miniaturized QCA with respect to α-stable noise is achieved.
- An impulsive noise-resilient QCA-FFT butterfly powered by the MCC criterion based equalization with OMP-based denoising is proposed to enhance the noise-robustness in the presence of stable-noise due to miniaturization.
- A MATLAB-based simulation environment for the noisy FFT-butterfly is developed to model circuit-level noise disturbances, implement the OMP/MCC-based denoising algorithm/channel-equalization, and perform performance-evaluation of Bit Error Rate (BER) of the proposed algorithm. Notably, we performed all operations using simulations of reversible QCA circuits, and their noisy variants. For our

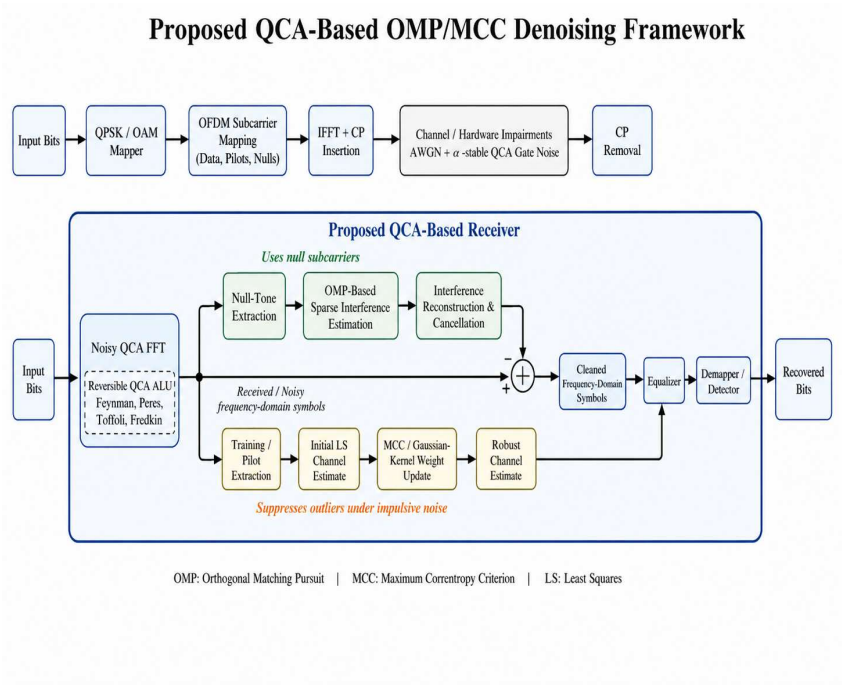


Fig. 1: Considered System Model.

noisy gate simulation, we assume an ALU that has adders, subtractors, and complex multipliers using QCA technology for DSP transform architectures using reversible QCA logic.

- Using QCA based FFT modules (or the said ALU), we present performance evaluations over IEEE 802.11a standard for indoor LAN, and LTE downlink and observe significant BER gains for the propsoed algorithm.

2 System Model

In this section, we present the system model for our FFT denoising that mitigates noisy QCA gates due to miniaturization. The architecture integrates MCC based denoising modules within the FFT pipeline to suppress error propagation between computational stages.

2.1 System Model with Noisy Reversible-Gate-Based FFT

2.1.1 OFDM Signal Model

Let the transmitted frequency-domain OFDM symbol be

$$X[k], \quad k = 0, \ldots, N-1, \quad N = 64. \tag{2}$$

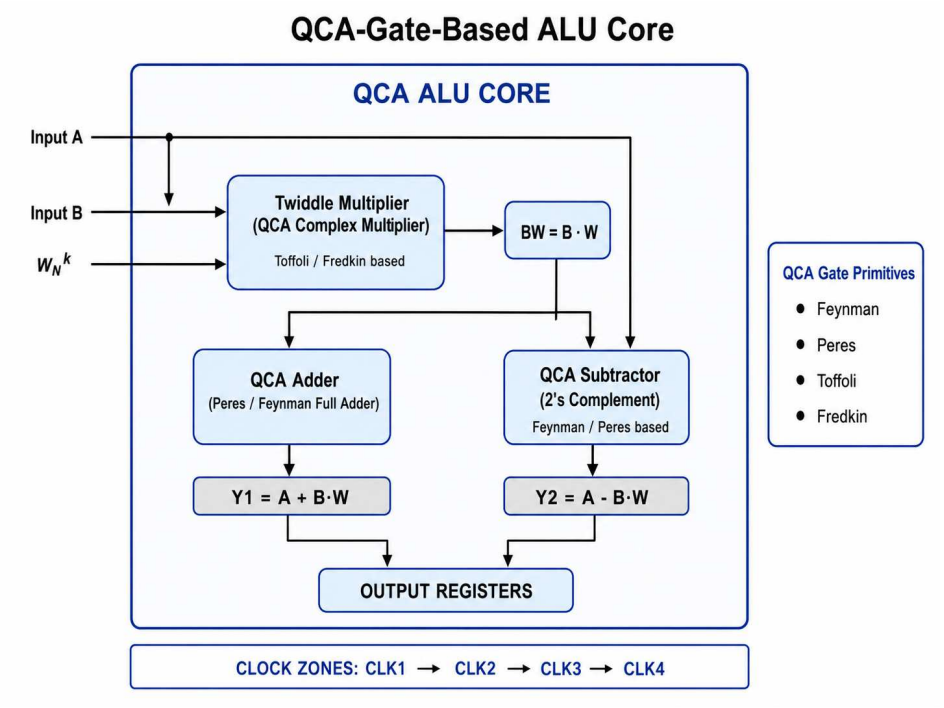


Fig. 2: Depiction of the proposed QCA based ALU

The time-domain signal is obtained via IFFT:

$$x[n] = \frac{1}{N} \sum_{k=0}^{N-1} X[k] e^{j2\pi kn/N}. \tag{3}$$

After cyclic prefix (CP) insertion and transmission over AWGN:

$$r[n] = x[n] + w[n], \tag{4}$$

where $w[n] \sim \mathcal{CN}(0, \sigma_w^2)$.

The receiver applies a noisy FFT:

$$Y[k] = \mathcal{F}_{\text{QCA,noisy}}\{r[n]\}. \tag{5}$$

2.2 Derivation of Max-Entropy Statistics for Noisy QCA Gates

This subsection justifies a simulation framework for modeling noise in QCA-based reversible circuits under cell-size-dependent coupling uncertainty. The reversible circuit is constructed from QCA primitive operations, namely majority logic, inversion, wire propagation, and XOR logic. These primitives are then used to realize Feynman, Toffoli, Fredkin, and Peres reversible gates.

The analog field at a QCA primitive output is modeled as

$$F = F_{\text{intended}} + F_{\text{parasitic}} + \eta,$$

where F_{intended} represents the designed QCA majority/inverter/wire interaction, $F_{\text{parasitic}}$ represents unintended neighboring-cell coupling, and η denotes local impulsive noise. The binary output is obtained using the polarization threshold rule

$$y = \begin{cases} 1, & F \geq 0, \\ 0, & F < 0. \end{cases}$$

The intended QCA majority gate is represented by normalized deterministic couplings

$$J_{1,2} = J_{1,3} = J_{1,4} = 1,$$

while parasitic neighboring couplings are modeled stochastically. To avoid imposing unnecessary distributional assumptions, the relative parasitic distances are sampled using a bounded maximum-entropy model:

$$r_k \sim \mathcal{U}(r_{k,\min}, r_{k,\max}).$$

The corresponding nominal parasitic coupling bounds are distance attenuated as follows (this assumption follows from the well-known semiconductor diffusion laws):

$$J_{\text{bound},k} = J_0 \exp\left(-\frac{r_k}{r_0}\right),$$

and the nominal parasitic coupling is drawn as

$$J_{1,k}^{(0)} \sim \mathcal{U}\left(-J_{\text{bound},k}, J_{\text{bound},k}\right), \qquad k = 5, \ldots, 10.$$

Cell-size effects are incorporated through a coupling scaling law. For a cell size d and baseline size d_0, the scaling factor is

$$m(d) = \frac{d_0}{d}.$$

The miniaturized parasitic coupling is then modeled as

$$J_{1,k}(d) = \text{clip}\left[J_{1,k}^{(0)} m(d)^2, -J_{\max}, J_{\max}\right].$$

The clipping operation prevents unphysical domination of the intended QCA logic by parasitic neighbors.

The local disturbance is modeled using a symmetric α-stable distribution:

$$\eta \sim S_{\alpha_\eta}\left(0, \gamma_\eta(d), 0\right),$$

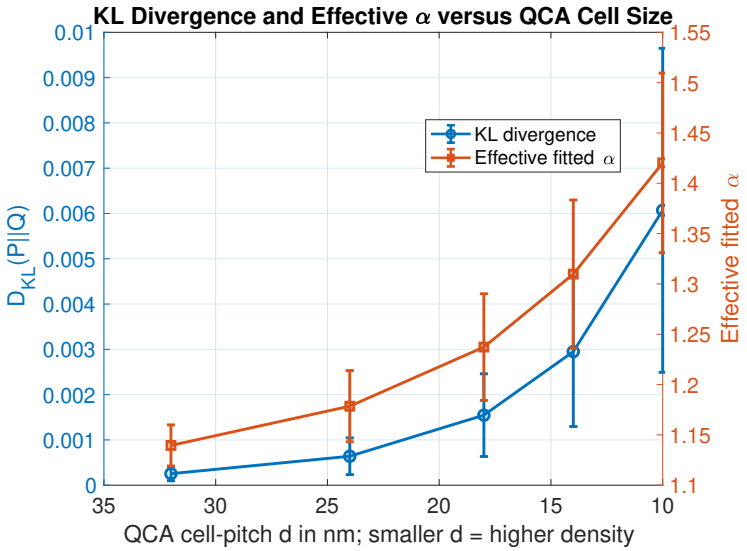


Fig. 3: KL DFivergence and Effective α vs QCA cell-size.

where α_η controls the impulsiveness of the local disturbance and $\gamma_\eta(d)$ is the scale parameter. The scale is allowed to vary with cell size according to

$$\gamma_\eta(d) = \min\left[\gamma_{\eta,0}\left(\frac{d_0}{d}\right)^{q_\gamma}, \gamma_{\eta,\max}\right].$$

Thus, stronger scaling or reduced cell size can increase the strength of impulsive local disturbances.

The resulting analog disturbance samples are collected from all QCA primitive operations. The empirical distribution of this disturbance is compared with candidate symmetric α-stable distributions using Kullback–Leibler divergence:

$$D_{\mathrm{KL}}(P\|Q) = \sum_i P_i \log\left(\frac{P_i}{Q_i}\right),$$

where P_i is the empirical histogram probability of the simulated QCA disturbance and Q_i is the fitted α-stable histogram probability. The effective circuit-level stability index is estimated as

$$\hat{\alpha} = \arg\min_{\alpha\in\mathcal{A}} D_{\mathrm{KL}}\left(P\|Q_\alpha\right),$$

where $\mathcal{A}$ is the candidate search grid for α. The validation of the assumption for impulsive noise is given in Fig. 3. It is observed that in the high pitch regime, the α-values come near unity and deviate from Gaussianity, which leads to more degradations. Furthermore, we can observe infinitesimal "best" KLD for $\alpha \in [1.1, 1.5]$, which shows the fit of the proposal α-stable distribution to the noise-data.

2.2.1 Noisy QCA Arithmetic Model

All arithmetic operations in the FFT are implemented using reversible logic and are affected by additive noise:

$$\tilde{z} = z + \nu, \quad \nu \sim S_\alpha(0, \gamma), \tag{6}$$

where S_α denotes a symmetric α-stable distribution.

Thus, any operation $\mathcal{O}(a, b)$ becomes

$$\tilde{\mathcal{O}}(a, b) = \mathcal{O}(a, b) + \nu. \tag{7}$$

2.2.2 Reversible Logic Gate Models

1) Feynman Gate (CNOT)

$$(a, b) \to (p, q) = (a, a \oplus b) \tag{8}$$

Noisy version:

$$\tilde{q} = a \oplus b + \nu_F. \tag{9}$$

2) Peres Gate

$$(a, b, c) \to (p, q, r) = (a, a \oplus b, ab \oplus c) \tag{10}$$

Noisy outputs:

$$\tilde{q} = a \oplus b + \nu_P, \quad \tilde{r} = ab \oplus c + \nu_P. \tag{11}$$

3) Toffoli Gate

$$(a, b, c) \to (a, b, c \oplus ab) \tag{12}$$

Noisy output:

$$\tilde{c} = c \oplus ab + \nu_T. \tag{13}$$

4) Fredkin Gate (Controlled Swap)

$$(c, a, b) \to (c, a', b') \tag{14}$$

where

$$(a', b') = \begin{cases} (b, a), & c = 1 \\ (a, b), & c = 0 \end{cases} \tag{15}$$

Noisy switching:

$$\tilde{a}', \tilde{b}' = (a', b') + \nu_{Fr}. \tag{16}$$

2.2.3 Reversible Arithmetic Construction

Addition (Ripple-Carry)

Using Peres gates:

$$s_i = a_i \oplus b_i \oplus c_i \tag{17}$$

$$c_{i+1} = a_i b_i \oplus c_i (a_i \oplus b_i) \tag{18}$$

Noisy addition:

$$\tilde{s}_i = s_i + \nu_{\text{add}}. \tag{19}$$

Multiplication (Twiddle Factor)

Using Toffoli-controlled partial products:

$$z = \sum_{k=0}^{W-1} b_k (a \ll k) \tag{20}$$

with noisy accumulation:

$$\tilde{z} = z + \nu_{\text{mul}}. \tag{21}$$

2.2.4 Noisy FFT Butterfly

For radix-2 FFT:

$$u = X[k] \tag{22}$$

$$t = W_N^j \cdot X[k + N/2] \tag{23}$$

Using noisy reversible arithmetic:

$$\tilde{t} = \tilde{\mathcal{M}}(W_N^j, X[k + N/2]) \tag{24}$$

$$\tilde{X}[k] = \tilde{\mathcal{A}}(u, \tilde{t}) \tag{25}$$

$$\tilde{X}[k + N/2] = \tilde{\mathcal{S}}(u, \tilde{t}) \tag{26}$$

where $\tilde{\mathcal{A}}, \tilde{\mathcal{S}}, \tilde{\mathcal{M}}$ denote add, subtract, multiply operations implemented via reversible gates.

2.2.5 End-to-End Model

The received FFT output can be written as:

$$Y[k] = X[k] + H_{\text{QCA}}(k) + W[k], \tag{27}$$

where

- $W[k]$ is channel noise,
- $H_{\text{QCA}}(k)$ is aggregate hardware-induced noise from reversible gates.

The QCA/reversible implementation introduces:

- Non-Gaussian, heavy-tailed arithmetic noise
- Stage-dependent noise accumulation
- Nonlinear distortion in FFT outputs

This motivates the use of **OMP/MCC-based denoising/equalization**, which is robust to non-Gaussian noise. In details, the MCC based denoising algorithm first forms a null-subcarrier sensing matrix by selecting the DFT rows corresponding to the null set. For each received OFDM symbol, it transforms the time-domain signal to

the frequency domain and extracts the null-tone observations. Since null tones ideally carry no data, any significant energy on them is treated as evidence of sparse impulsive interference. OMP is then applied by iteratively selecting the time-domain index most correlated with the current null-tone residual, updating the support set, estimating the impulse amplitudes using least squares, and refining the residual. After the OMP iterations, the estimated sparse interference vector is reconstructed and subtracted from the received time-domain OFDM symbol. The cleaned signal is then transformed back to the frequency domain. Next, for each data subcarrier, the cleaned training observations are collected and an initial least-squares channel estimate is computed. This channel estimate is refined using Gaussian-kernel MCC based weighting, where samples with large residual errors receive smaller weights and therefore contribute less to the estimate. Finally, the cleaned payload symbols are equalized using the refined channel estimate and then demodulated to recover the transmitted bits. The proposed algorithm is summarized in **Algorithm 1**.

Algorithm 1 Null-Aided OMP Denoising With MCC based Equalization

Require: $\mathbf{r}_k$, null set $\mathcal{N}$, data set $\mathcal{D}$, training symbols $\mathbf{x}_m^{\mathrm{tr}}$, DFT matrix $\mathbf{F}$
Ensure: Equalized payload symbols $\hat{X}_{m,k}$

$\mathbf{A}_{\mathcal{N}} = \mathbf{F}(\mathcal{N}, :)$
for $k = 1, \ldots, N_s$ **do**
  $\mathbf{Y}_k = \mathbf{F}\mathbf{r}_k, \quad \mathbf{y}_{\mathcal{N},k} = \mathbf{Y}_k(\mathcal{N})$
  Initialize $\mathbf{e}_k = \mathbf{y}_{\mathcal{N},k}$ and $\mathcal{S} = \emptyset$
  for $i = 1, \ldots, K_{\max}$ **do**
    $n^\star = \arg\max_n |\mathbf{a}_n^H \mathbf{e}_k|$
    $\mathcal{S} \leftarrow \mathcal{S} \cup \{n^\star\}$
    $\hat{\boldsymbol{\alpha}} = \arg\min_{\boldsymbol{\alpha}} \|\mathbf{y}_{\mathcal{N},k} - \mathbf{A}_{\mathcal{N},\mathcal{S}}\boldsymbol{\alpha}\|_2^2$
    $\mathbf{e}_k \leftarrow \mathbf{y}_{\mathcal{N},k} - \mathbf{A}_{\mathcal{N},\mathcal{S}}\hat{\boldsymbol{\alpha}}$
  end for
  Construct $\hat{\mathbf{i}}_k$ from $\mathcal{S}$ and $\hat{\boldsymbol{\alpha}}$
  $\tilde{\mathbf{r}}_k = \mathbf{r}_k - \hat{\mathbf{i}}_k, \quad \tilde{\mathbf{Y}}_k = \mathbf{F}\tilde{\mathbf{r}}_k$
end for
for each $m \in \mathcal{D}$ **do**
  Collect $\mathbf{y}_m^{\mathrm{tr}}$ from $\tilde{\mathbf{Y}}_k$
  $\hat{H}_m = \dfrac{(\mathbf{x}_m^{\mathrm{tr}})^H \mathbf{y}_m^{\mathrm{tr}}}{(\mathbf{x}_m^{\mathrm{tr}})^H \mathbf{x}_m^{\mathrm{tr}}}$
  for $t = 1, \ldots, T$ **do**
    $\boldsymbol{\varepsilon} = \mathbf{y}_m^{\mathrm{tr}} - \hat{H}_m \mathbf{x}_m^{\mathrm{tr}}$
    $w_\ell = \exp\left(-|\varepsilon_\ell|^2/(2\sigma^2)\right)$
    $\hat{H}_m = \dfrac{(\mathbf{x}_m^{\mathrm{tr}})^H \mathbf{W} \mathbf{y}_m^{\mathrm{tr}}}{(\mathbf{x}_m^{\mathrm{tr}})^H \mathbf{W} \mathbf{x}_m^{\mathrm{tr}}}$
  end for
  $\hat{X}_{m,k} = \tilde{Y}_{m,k}/(\hat{H}_m + \epsilon)$
end for
Demodulate $\hat{X}_{m,k}$.

3 Simulations

In this section, we present simulations to validate the proposed FFT-butterfly with MCC based denoising in the presence of stable noise due to nanoscale phenomena like leakage, and other artefacts due to miniaturization. Within the QCA framework, we considered an IEEE OFDM 802.11a LAN standard and higher order LTE standards such as 128,512, 1024 and 2048 based LTE downlink systems for our simulation-study, and plotted the BER using: a) FFT-butterflies with no denoising, and b) FFT-butterflies using OMP/MCC based denoising/equalization, assuming noisy gates defined in the previous sections. The simulation parameters are tabulated in Table. 1.

Table 1: Simulation Parameters

Parameter	**Value**
OFDM size, N	64,128,512,1024
Cyclic prefix length, N_{CP}	16
Training modulation	QPSK, $M_{\mathrm{tr}} = 4$
Payload modulation	16,64-QAM, $M_{\mathrm{data}} = 16, 64$
Number of OFDM symbols	70000
Number of training symbols, N_{tr}	160
Number of data symbols	69840
Active subcarriers	$[-26 : -1,\ 1 : 26]$
Pilot subcarriers	$[-21,\ -7,\ 7,\ 21]$
Data subcarriers	48 (for 64-OFDM)
Null subcarriers	DC and guard-band tones
Pilot symbols	$[1,\ 1,\ 1,\ -1]^T$
FFT/IFFT normalization	$\mathbf{F}/\sqrt{N},\ \sqrt{N}\mathbf{F}^{-1}$
Heavy-tailed noise parameter, α	1
QCA-like noise base	3.0×10^{-2}
Maximum OMP atoms, $K_{\max}$	4
OMP stopping factor	1.15
Minimum null energy threshold	10^{-14}
MCC scale factor	2.0
Kernel iterations	13
Kernel floor value	10^{-10}
Baseline receiver	No impulse cancellation + LS equalization
Proposed receiver	Null-aided OMP cancellation + MCC based equalization

In Fig. 4, it is observed that the proposed usage of QCA based FFT-butterfly with OMP/MCC based denoising/equalization converges to a lower BER compared to a generic QCA based FFT-butterfly without any denoising in the presence of α-stable noise with $\alpha = 1$, which makes the proposed algorithm attractive for QCA-FFT. This trend is observed in Fig. 4 for $\alpha = 1, 1.5$ and for modulations 16, 64-QAM.

Next, within the same QCA framework, benefits are observed in Fig. 5 as we vary the OFDM order to 128, 512, 1024, and 2048 assuming an LTE downlink, for α-stable

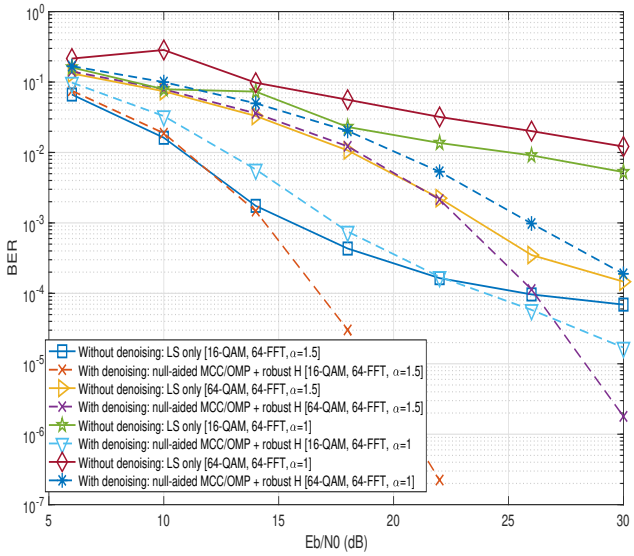


Fig. 4: Performance Evaluation of BER for 16 QAM and 64 QAM in α-stable noise with $\alpha = 1, 1.5$ in IEEE 802.11a WLAN standard with 64 subcarriers.

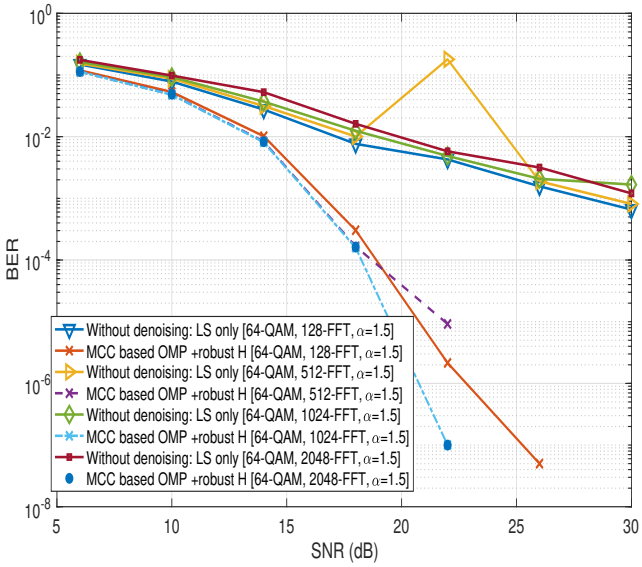


Fig. 5: Performance Evaluation of BER for higher order QAM in LTE downlink, with 128,512,1024 and 2048 carriers assuming $\alpha = 1.5$.

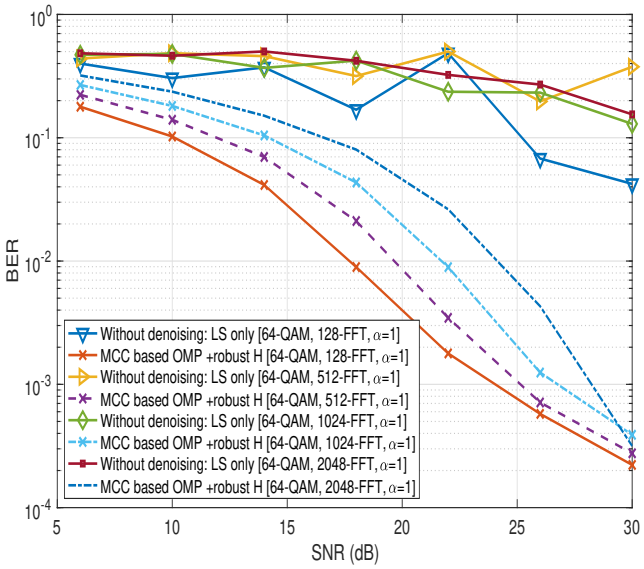


Fig. 6: Performance Evaluation of BER for higher order QAM in LTE downlink, with 128,512,1024 and 2048 carriers assuming $\alpha = 1$.

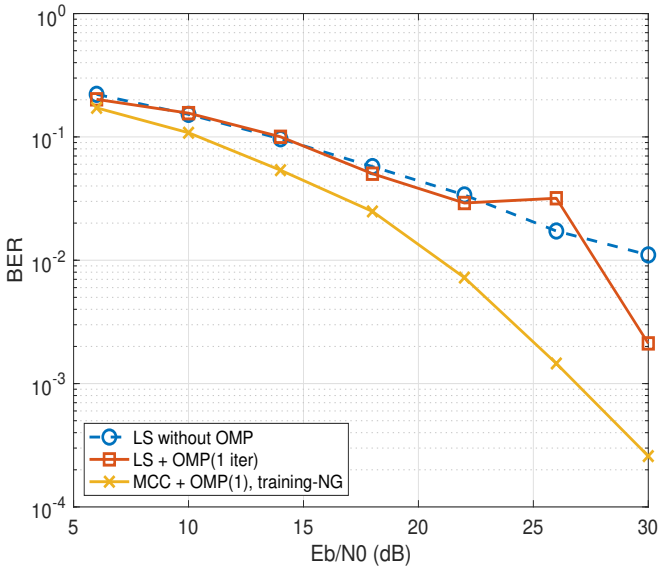


Fig. 7: Justification for the use of MCC based equalization as opposed to LS based denoising for imperfect OMP.

noise with $\alpha = 1.5$. Similar performance gains in BER for various OFDM orders is observed in Fig. 6 for $\alpha = 1$.

Lastly, in Fig. 7, we provide the justification of choosing the proposed MCC based equalization in conjunction with OMP instead of LS based equalization with OMP. For achieving computational simplicity, we sometimes choose lesser number of OMP-atoms for approximating the additive inference. This leads to a residual non-Gaussian additive term, which is better-mitigated by MCC based equalization in the second stage instead of LS in the second stage. In Fig. 7, we observe that the two-stage OMP+MCC outperforms OMP+LS and LS without OMP assuming a hypothetical 1-atom OMP dictionary based imperfect OMP, from which the viability of OMP/MCC based denoising/equalization is inferred for impulse noise impaired QCA circuits.

4 Conclusion

In this paper, using reversible QCA gates enhanced by ITL, we presented the performance evaluation of FFT based communication systems applications like IEEE 802.11 LAN OFDM, and LTE downlink with large OFDM order in presence of non-Gaussian noises. Through analytical results, we first noted the convergence of noise in QCA gates to stable distributions. Next, the propagation of noisy gates in FFT applications was demonstrated and MCC based denoising was proposed to mitigate the stable noise. The presented simulations indicate significant performance improvements for the MCC based denoising algorithm applied on FFT/IFFT blocks for realistic OFDM applications. This makes the MCC based denoising algorithm viable for deployment over miniaturized QCA based FFT blocks for OFDM.

5 Data Availability Statement

Data sharing is not applicable to this article as no datasets were generated or analyzed during the current study.

References

[1] Moore, G.E., et al.: Cramming more components onto integrated circuits. McGraw-Hill New York (1965)

[2] Ionescu, A.M., Riel, H.: Tunnel field-effect transistors as energy-efficient electronic switches. nature **479**(7373), 329–337 (2011)

[3] Association, S.I., et al.: ITRS: International technology roadmap for semiconductors (2009)

[4] Lent, C.S., Tougaw, P.D., Porod, W., Bernstein, G.H.: Quantum cellular automata. Nanotechnology **4**(1), 49–57 (1993)

[5] Lent, C.S., Tougaw, P.D.: A device architecture for computing with quantum dots. Proceedings of the IEEE **85**(4), 541–557 (2002)

[6] Landauer, R.: Irreversibility and heat generation in the computing process. IBM journal of research and development **5**(3), 183–191 (1961)

[7] Bennett, C.H.: Logical reversibility of computation. IBM journal of Research and Development **17**(6), 525–532 (1973)

[8] Frank, M.P.: Introduction to reversible computing: motivation, progress, and challenges. In: Proceedings of the 2nd Conference on Computing Frontiers, pp. 385–390 (2005)

[9] Sathya, V., Shakunthala, M., Chakravarthy, V., Radhika, K., Rao, G.N., Jagtap, M.T., Ramya, E., Bani, S.G.: Radial basis convoluted graph neural network based area efficient 1024-point pipelined radix4 FFT processer for ECG heartbeat categorization. Circuits, Systems, and Signal Processing **45**(2), 1318–1347 (2026)

[10] Abdoli, H., Nikmehr, H., Movahedinia, N., De Dinechin, F.: Improving energy efficiency of OFDM using adaptive precision reconfigurable FFT. Circuits, Systems, and Signal Processing **36**(7), 2742–2766 (2017)

[11] Agarwal, S., Ahamed, S.R., Gogoi, A., Trivedi, G.: A 28-gbps radix-16, 512-point FFT processor-based continuous streaming ofdm for WiGig. Circuits, Systems, and Signal Processing **41**(5), 2871–2897 (2022)

[12] Dongye, G., Ding, M., Cao, J., Tang, B., Ding, Y.: Generalized fractional fourier transform-based target localization by doppler radar. Circuits, Systems, and Signal Processing, 1–24 (2026)

[13] Sindhu, R., Arunachalam, V.: Design of an approximate radix-2 FFT butterfly unit for lstm-speech signal-based parkinson's disease classifier. Circuits, Systems, and Signal Processing **44**(6), 4258–4278 (2025)

[14] Lin, H.-J., Shen, C.-A.: The architectural optimizations of a low-complexity and low-latency FFT processor for MIMO-OFDM communication systems. Journal of Signal Processing Systems **93**(1), 67–78 (2021)

[15] Lin, Y.-C., Lee, T.-S., Lin, C.-H.: Interference avoidance and cancellation in automotive OFDM radar networks. Journal of signal processing systems **92**(12), 1383–1396 (2020)

[16] Bhatia, V., Mulgrew, B., Falconer, D.D.: Non-parametric ML channel estimator and detector for OFDM. In: 2005 13th European Signal Processing Conference, pp. 1–4 (2005). IEEE

[17] Principe, J.C.: Information Theoretic Learning: Renyi's Entropy and Kernel Perspectives. Springer, ??? (2010)

[18] Orlov, A.O., Amlani, I., Toth, G., Lent, C.S., Bernstein, G.H., Snider, G.L.:

Experimental demonstration of a binary wire for quantum-dot cellular automata. Applied physics letters **74**(19), 2875–2877 (1999)

[19] Walus, K., Dysart, T.J., Jullien, G.A., Budiman, R.A.: Qcadesigner: A rapid design and simulation tool for quantum-dot cellular automata. IEEE transactions on nanotechnology **3**(1), 26–31 (2004)

[20] Tahoori, M.B., Huang, J., Momenzadeh, M., Lombardi, F.: Testing of quantum cellular automata. IEEE Transactions on Nanotechnology **3**(4), 432–442 (2004)

[21] Lent, C.S., Isaksen, B.: Clocked molecular quantum-dot cellular automata. IEEE Transactions on Electron Devices **50**(9), 1890–1896 (2003)

[22] Bhanja, S., Sarkar, S.: Probabilistic modeling of QCA circuits using bayesian networks. IEEE Transactions on Nanotechnology **5**(6), 657–670 (2006)

[23] Gnedenko, B.V., Kolmogorov, A.N.: Limit Distributions for Sums of Independent Random Variables. Addison-Wesley, Cambridge, MA (1954)